Measurement Science
and Technology

PAPER • **OPEN ACCESS**

Terrestrial laser scanners and contrast targets: effect of algorithm, resolution, distance, and target rotational orientation on center coordinate

To cite this article: Bala Muralikrishnan *et al* 2026 *Meas. Sci. Technol.* **37** 285002

IOP Publishing Meas. Sci. Technol. 37 (2026) 285002 https://doi.org/10.1088/1361-6501/ae7f3c

Measurement Science and Technology

OPEN ACCESS

RECEIVED
24 March 2026

REVISED
11 May 2026

ACCEPTED FOR PUBLICATION
18 June 2026

PUBLISHED
13 July 2026

PAPER

Terrestrial laser scanners and contrast targets: effect of algorithm, resolution, distance, and target rotational orientation on center coordinate

Bala Muralikrishnan[1,*], **Aum Shah**[1,2], **Mary Gregg**[3], **Meghan Shilling**[1], **Vincent Lee**[1] and **Braden Czapla**[1]

[1] Sensor Science Division, National Institute of Standards and Technology, Gaithersburg, MD 20899, United States of America
[2] Academy for Mathematics, Science and Engineering, Rockaway, NJ 07866, United States of America
[3] Statistical Engineering Division, National Institute of Standards and Technology, Boulder, CO 80305, United States of America
[*] Author to whom any correspondence should be addressed.

E-mail: balam@nist.gov

Keywords: center error, contrast target, orientation, scan density, terrestrial laser scanner

Abstract

Terrestrial laser scanners (TLSs) are portable dimensional measurement instruments that produce a 3D point cloud by measuring the distance and two angles to points in the scene. Contrast targets are sometimes used to evaluate the performance of these scanners by comparing inter-target distances to measurements made using higher accuracy instruments or to register scans from different positions of the TLS. The choice of algorithm, distance of the target from the TLS, scan resolution, and rotational orientation of the target contribute to errors in the target center coordinates. We explored this problem using an artifact consisting of spheres and a contrast target that allowed us to monitor the center of the contrast target in a coordinate system established using the spheres, where the assumption is that the sphere centers are unaffected by factors mentioned earlier and therefore provide a stable coordinate system. We considered three different TLSs and four algorithms to detect contrast target center (three custom developed and one from the manufacturer). For each TLS, we performed scans at two distances, two resolutions, and three rotational orientations of the target, for a total of 12 cases (with 10 repeated scans per case, total of 120 scans). We calculated two response variables for each case—inter-case variation d and intra-case variation s. For TLS A, low resolution scans produced the worst results (large d and s values) for the original equipment manufacturer (OEM) algorithm, with d and s as large as 2 and 0.3 mm, respectively, for one of the cases. For TLS B, target orientation of 90° produced the worst results for the OEM algorithm, with d and s as large as 2 and 1.3 mm, respectively, for certain cases. For TLS C, only the far distance, low resolution, and 90° target orientation case produced the worst result for the OEM algorithm, with d and s values as large as 0.3 and 0.6 mm, respectively. Our custom algorithms clearly outperformed the OEM algorithms for TLS A and B and while the OEM algorithm marginally outperformed the custom algorithms for TLS C.

1. Introduction

Terrestrial laser scanners (TLSs) [1, 2] are spherical coordinate dimensional measurement instruments that produce a 3D point cloud by recording the range and two angles of points on the surfaces of objects in the scene. They are portable and are therefore extensively used in many indoor as well as outdoor applications such as in construction [3, 4], deformation monitoring [5, 6], mining [7], cave [8], tunnel [9], and bridge [10] surveying, forest monitoring [11], cultural heritage preservation and modeling [12], crime and accident scene reconstruction [13], ship building [14], etc.

The significant benefit of TLSs when compared to laser trackers or some total stations is that TLSs can obtain data from objects in the scene without the need to use special cooperative targets at each

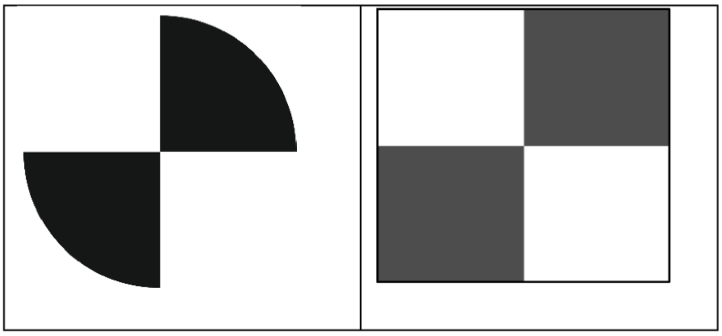

Figure 1. Contrast target with alternating black and white geometries.

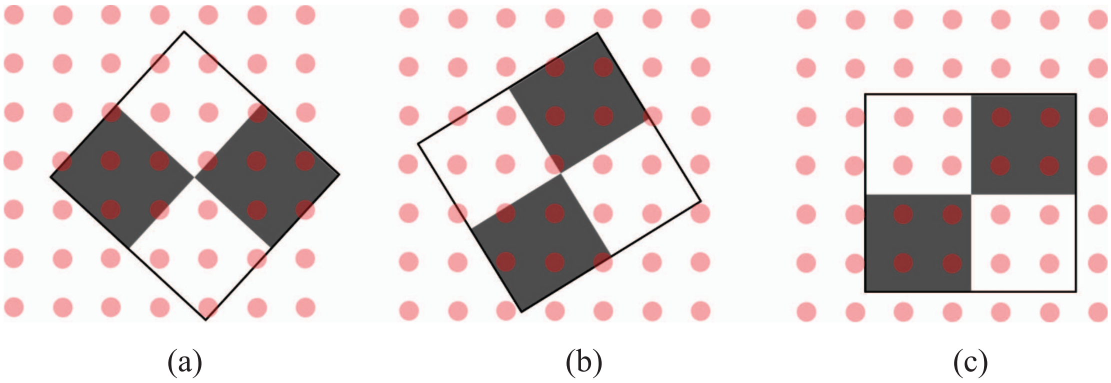

Figure 2. Target oriented at roll angles of (a) 45°, (b) 67°, (c) 90°. Laser spots are shown as filled red circles. Some points lie on the transition lines in (a) and (b). In (c), the transition lines are entirely between scan columns and rows. Note that the size of the red dots in the figure depends on the distance of the target from the TLS while the spacing depends on the distance and the resolution of the scan.

point of interest. While cooperative targets are not necessary, other types of targets are sometimes used to either evaluate the performance of the TLS by comparing inter-target distances to measurements made using higher accuracy instruments (such as a laser tracker) or to register scans from different positions of the TLS. Contrast targets (also referred to as checkerboard targets), see figure 1, are commonly used for this purpose as they are inexpensive and can be easily procured. Because a contrast target is two-dimensional as opposed to a sphere, the target position and orientation, in conjunction with the algorithm employed to detect the center, can introduce errors, see [15].

In [15], the authors considered the effect of target pitch and yaw rotations on the center coordinate (see section 2 for more on this). In this work, we consider the effect of target roll on the center coordinate. Roll is the rotational orientation in the plane of the target. Three different roll angles are shown in figure 2. The underlying hypothesis for this work is that the roll orientation in combination with the sparsity of the data set and the algorithm employed can affect center coordinates. The reasoning is straightforward. TLS collects data in vertical columns. If a target is arranged as shown in figures 2(a) and (b), a large target will register some points within each square and some points in the transition region between the black and white portions, potentially allowing for a more accurate center estimation. If a target is arranged as in figure 2(c), the lines of a scan column or row can completely miss the transition region resulting in errors in the center location. This problem is exacerbated at low resolutions and far distances.

The algorithm used to detect the center is an important factor in this study. There is only some literature available on this topic. An edge-based technique was proposed in [16] and later in [17, 18]. The technique involved identifying points whose intensities are mid-way between the black and the white portions, as they represent the points in the transition region. This was followed by fitting lines to those points and determining the intersection. A method based on correlation was presented in [19] where they match an input image within a search window but do not use a pre-defined mask, instead the mask was the region of interest rotated by 180°. This method required that the region around the center remain symmetric. A similar approach where a mask is matched with the measured data was presented in [20]. Unlike the case in [19] where the measured data rotated by 180° was used as the mask, here, an orthographic image of a typical target was used as a mask to match the intensity image of the target to determine center. An approach based on Morse theory was presented in [21] where the intensity is transformed to surface height and saddle points are extracted to detect target center. They claim higher precision in the target centers than the scanning resolution. A geometric method to determine the target center with higher precision was reported in [22]. They estimated various parameters from the point cloud which they then used to determine the variant of the target center calculations to choose from. They showed that their approach can reduce errors by up to 6 mm compared to conventional automatic methods. A technique based on template matching was described in [23] where a model of the target, including intensity information, was fit to the point cloud to find the center of the target. A review of different algorithms and a comparison of their performance can be found in [24]. In this paper, we consider three custom developed algorithms in addition to the manufacturer-provided algorithm. One of the custom algorithms is an edge-based technique while the other two are area-based techniques. They are described in section 3.

The motivation for the work described in this paper is an ongoing documentary standards effort within the Crime Scene Investigation and Reconstruction subcommittee (CSIR) of the Organization for Scientific Activities in Forensics (OSAC) [25]. This subcommittee is currently developing an interim performance assessment procedure for TLSs [26, 27] that use contrast targets. To better inform the committee on optimal placement of targets, it is necessary to understand the effect of factors such as target orientation, scan resolution, and distance, on target induced errors. The work described in this paper is a step in that direction. This is particularly important because these targets are frequently employed in registering multiple scan data into a single 3D point cloud. Errors in locating target centers can accumulate leading to large errors in the overall point cloud. Further, as mentioned earlier, these targets are also sometimes used to evaluate the performance of TLSs. Errors in target centers might be attributed to poor TLS performance when in fact the TLS is performing normally. Quantifying target center errors is therefore important in a number of domains such as construction, surveying, forensics, manufacturing, etc., where TLSs are increasingly used. The rest of this paper is organized as follows. We describe the approach in section 2, the algorithms used in section 3, present results in section 4, and conclude with a discussion in section 5.

2. Approach

We evaluated the errors in the contrast target centers using the artifact shown in figure 3. We described the artifact in an earlier work [15]. While we previously built the artifact to allow for pitch (about the X axis) and yaw (about the Y axis) rotations, we have since modified the artifact to allow for roll rotations (about the Z axis). The artifact is comprised of four 100 mm diameter spheres made of aluminum with a dull gray finish, and sphericity better than 10 μm. A contrast target, made using a laser printer and cardstock paper, is glued onto a flat aluminum plate, which is bolted to the breadboard on which the spheres are also mounted. The breadboard is mounted onto a single rotation stage to allow orientations about the Z axis as shown in figure 4 to be presented to the TLS. We positioned the contrast target in three roll orientations: 45°, 67°, and 90° degrees. The flatness of the target is limited by the flatness of the aluminum plate and the process of gluing the paper onto the plate. Scan data from a high accuracy TLS indicates the flatness of the target is about 0.3 mm. As we will see in the results section, this flatness is comparable to the magnitude of the errors in the center coordinate we are observing. However, the flatness of the paper has a second-order effect on the center errors because we are only interested in the movement of the center *in the plane* of the target, not perpendicular to the plane of the target. That is, we are focusing on the errors along the X and Y direction, not along Z, in figure 3. We have not considered the effect of the optical properties of the contrast target surface in this paper.

From the scan data of this artifact, we established a coordinate system using spheres A, B, and C (origin located at center of sphere A, center of sphere B on the X axis, and center of sphere C on the XY plane), and then evaluated the center of sphere D and the center of the contrast target in that coordinate system. Because a sphere appears spherical from any viewpoint, we expect the coordinate system established using the spheres to not be influenced by the orientation of the artifact. To evaluate the validity of our coordinate system, we compared the range of values of the coordinate of sphere D in our established coordinate system for the different cases (see table 1) with range of values of the coordinate of the contrast target. If the range of the contrast target coordinates is significantly larger than for sphere D (especially along X and Y) for the different cases considered, we can conclude that the contrast target suffers from errors due to the algorithm and/or distance/resolution/orientation combinations.

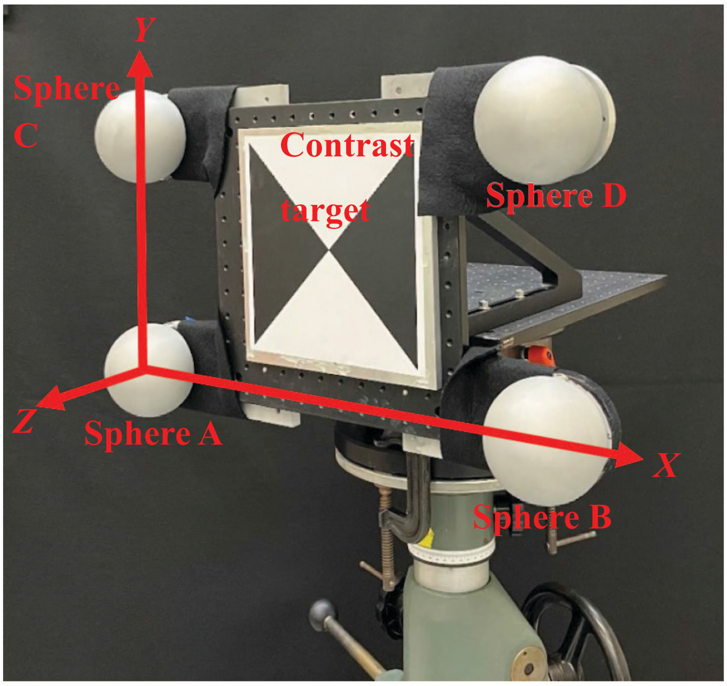

Figure 3. Artifact comprising four spheres and a contrast target to study errors as a function of orientation.

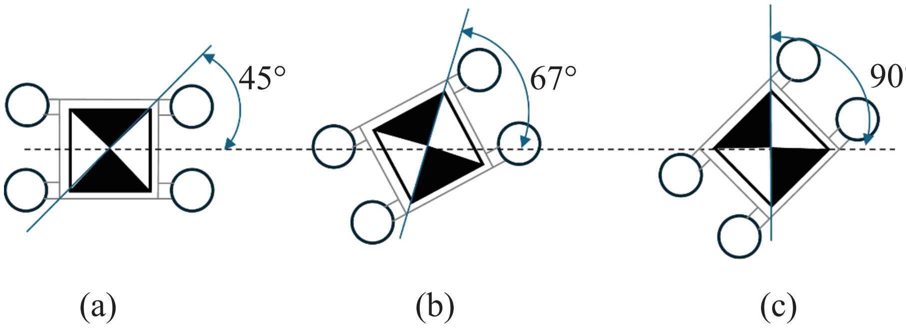

Figure 4. Different roll orientations of the artifact, (a) 45°, (b) 67°, (c) 90°. The TLS is located directly in front of the target, at target height, at either 5 or 10 m distance.

Table 1. Different cases considered (10 scans were performed for each case).

		Resolution (ppd)		
Case	Distance (m)	TLS A/B	TLS C	Target roll orientation (°)
1	5	28	30	45
2	10	28	30	45
3	5	109	90	45
4	10	109	90	45
5	5	28	30	67
6	10	28	30	67
7	5	109	90	67
8	10	109	90	67
9	5	28	30	90
10	10	28	30	90
11	5	109	90	90
12	10	109	90	90

We performed measurements on our artifact using three TLSs. One was a long-range (maximum range of more than 1 km) lower-accuracy TLS (TLS A) based on a time-of-flight range measurement system, one was a short range (~25 m) high-accuracy TLS based on a combination of time-of-flight and

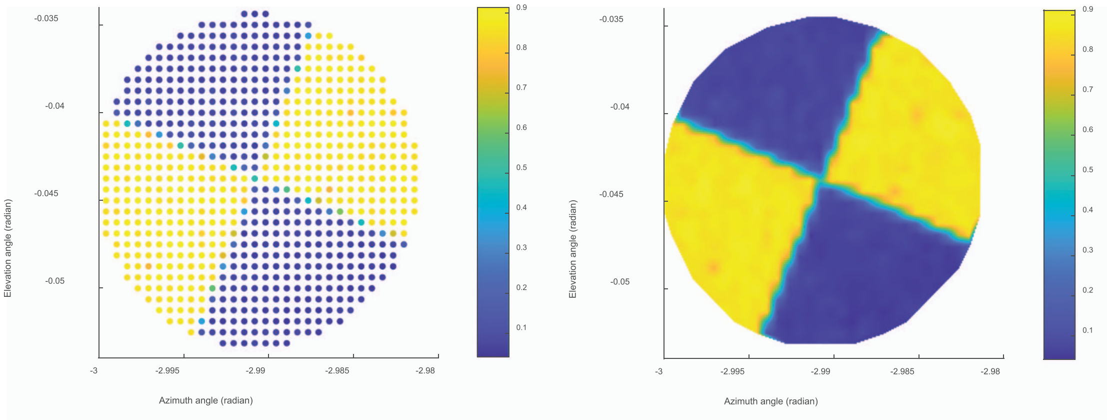

Figure 5. Intensity (in color) as a function of the azimuth and elevation angles for one of the TLSs at the 10 m distance, 28 ppd resolution, 67° target orientation for the (a) measured data, (b) interpolated data.

phase-shift range measurement system (TLS B), and the third was a short range (∼25 m) high-accuracy TLS based on a phase-shift range measurement system (TLS C). These three TLSs effectively represent the majority of TLSs used in the field today.

For each TLS, we performed the following scans. With the artifact about 5 m away from the TLS, and the TLS resolution set at a certain value, we performed 10 scans at each of three nominal target roll orientations: 45°, 67°, and 90° (30 total scans). We then changed the resolution and repeated the scans. We next moved the artifact to about 10 m from the TLS and repeated the scans for both resolutions. A total of 120 scans per TLS were thus acquired as seen below:

$$n_s = n_d \times n_{res} \times n_{to} \times n_{rep} = 2 \times 2 \times 3 \times 10 = 120, \quad (1)$$

where n_s is the total number of scans for each TLS, n_d is the number of distances, n_{res} is the number of resolutions, n_{to} is the number of target orientations, and n_{rep} is the number of repeats considered.

The different cases considered are listed in table 1. Regarding the choice of resolutions selected for the experiments, we chose one value at the lower end and one value at the higher end of the range of resolutions allowed for that TLS. From the options available, we choose 28 points-per-degree (ppd) and 109 ppd for TLSs A and B. From the options available, we choose 30 ppd and 90 ppd for TLS C.

We segmented each scan point cloud into five parts: each of the four spheres and the contrast target. The contrast target center was then found using the original equipment manufacturer (OEM) software for each scanner and also using our custom algorithms. We then transformed all centers into a coordinate system established using the centers of spheres A, B, and C.

3. Algorithms employed

In this study, we considered contrast target centers from four algorithms—three custom and one from the software provided by the manufacturer. The three algorithms that we implemented are described here. These operate in the T–P–I domain, where T is the azimuth angle, P is the elevation angle, and I is the intensity. Figure 5(a) shows the intensity (in color) as a function of the azimuth and elevation angles for the measured data for one of the TLSs at the 10 m distance, 28 ppd resolution, 67° target orientation. There are only about 730 points in the plot, which corresponds to a grid of about 30 × 30. There are not enough points in the transition regions (intensities around 0.4–0.6) to detect the edges. Because the highest density data we collected (5 m distance and 109 ppd resolution) encompassed a grid that was almost 250 × 250 points, we interpolate all data using natural neighbor interpolation to a 250 × 250 grid; such a grid is shown in figure 5(b) for the data in figure 5(a) where the transition regions are more clearly defined. We use such 2D interpolated point cloud in the following algorithms.

3.1. Edge method

We first identified edge points whose intensities were within $\pm 0.5\sigma$ of the mean intensity, where σ is the standard deviation. We separated the edge points into four quadrants and combined points in non-adjacent quadrants, resulting in the red and blue points in figure 6(a). We fit a line through the red

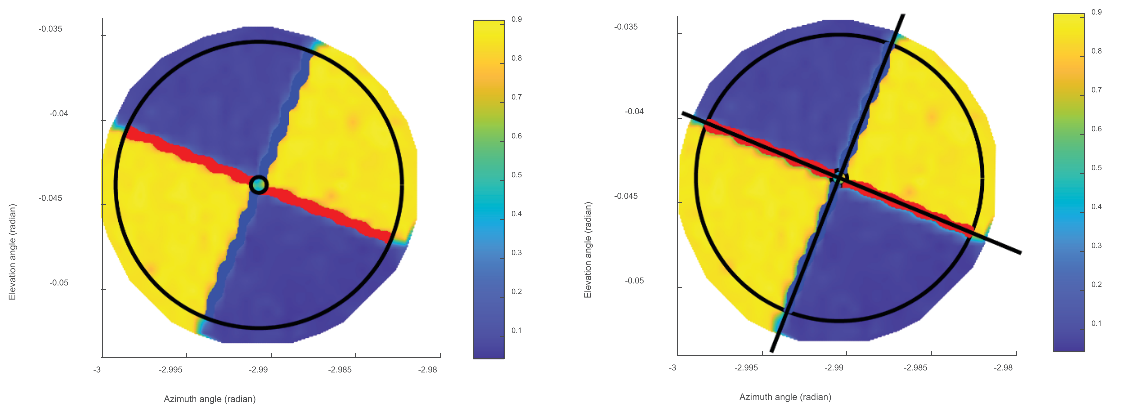

Figure 6. Intensity as a function of angle along with (a) edge points and concentric circles that define the region of interest (b) edge points, concentric circles, and least-squares best fit lines.

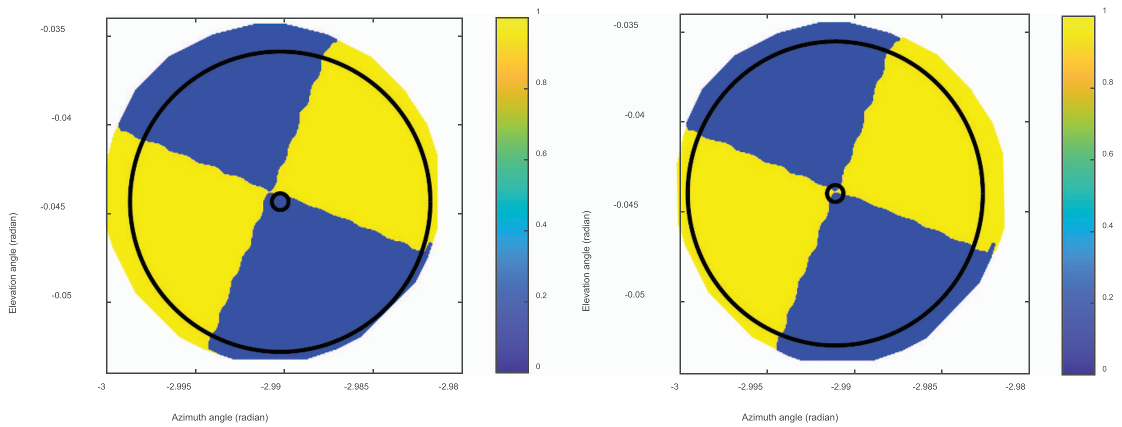

Figure 7. Binary point assignment based on k-means and concentric circles for the case where the circles are (a) offset, (b) centered.

points and another line through the blue points and determined the intersection point. Using this initial center, we extracted the region of the target that was within two concentric circles (shown in figure 6), again identified the edge points, fit lines, and found an updated center, (t,p). The purpose of the concentric circles is to eliminate points near the center of the target and near the edges where there may be mixed pixels that could potentially introduce errors. The radius of the inner and outer circles are parameters that are chosen based on target size.

3.2. Centroid method

We used k-means clustering to pre-assign points on the targets as belonging to the 'low' intensity region or the 'high' intensity region of the target. Thus, each point had a binary assignment, either 0 or 1, based on intensity. We then moved the two concentric circles described earlier using a minimization process so that the centroid (in the T–P plane) of the 'high' and 'low' intensity points in the region defined between the circles was as close as possible. The resulting center of the circles, (t,p) is considered the center of the target. Figure 7(a) shows the binary assignment of points for the interpolated data in figure 5(b). The blue region has an assigned k-means value of 0 while the yellow region has an assigned value of 1. The concentric circles are intentionally offset in this figure. If we consider the region between the circles, the blue region is not balanced, i.e. there are more blue points to bottom and right than there are in the top and to the left. Figure 7(b) shows the concentric circles centrally placed so that the blue and the yellow regions are balanced. All points in the region of interest (i.e. between the concentric circles) contribute to the identification of the center whereas in the edge method, it is only the points in the transition region that contribute to the center.

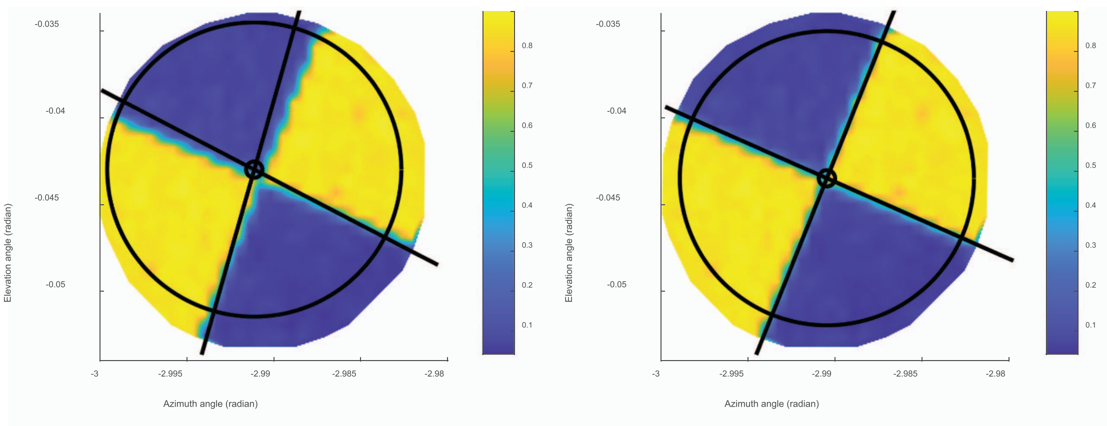

Figure 8. Intensity as a function of angle along with concentric circles and edge lines for the case where the circles are (a) offset, (b) centered.

3.3. Intensity method

We identified two lines that divide the target into four regions. We combined two non-adjacent regions to reduce the four to two regions. We calculated the mean intensity in each region and the deviations from the mean for all points in that region. We then calculated the sum of squared deviations. We translated and rotated the lines so that the sum of squared deviations was as small as possible. Figure 8(a) shows a starting guess for the two lines and the resulting four regions. Here, the two predominantly yellow regions also include several points from the blue regions, thus resulting in a larger sum of squared deviation. After the lines have been adjusted as shown in figure 8(b), the yellow and blue regions are segregated so that the sum of squared residuals is as small as possible. As before, we only considered data within a region of concentric circles whose radius had been previously established. The center of the circles is always kept coincident with the point of intersection of the lines.

4. Results

As mentioned in section 2, for each TLS, we performed 10 repeated scans for each of the 12 different cases listed in table 1. From each scan, we calculated the center coordinates for the two objects (sphere and contrast target). The sphere center coordinates were obtained by fitting a least-squares best-fit sphere to the point cloud. The contrast target center coordinates were obtained using each of the four algorithms (three custom algorithms and the OEM software). To assess whether the distance/resolution/orientation and/or the algorithm affects the center coordinates, we calculated two response variables, inter-case variation d and intra-case variation s, from the data. As the names suggest, response variable d is a measure of the variation in the center coordinates across the 12 different cases listed in table 1 while response variable s is a measure of the variation in the center coordinates within the 10 replicates of a given case. The rationale for the selection of these two variables lies in the need to distinguish systematic effects from random effects. The variable, s, captures the variation in the 10 replicates for a given case, it can therefore be viewed as an estimate of random effects. The variable, d, captures the variation between the cases, it can therefore be viewed as an estimate of systematic effects. We describe the calculation of the two response variables in section 4.1.

We present results for each TLS in sections 4.2–4.4 where we tracked the response variables d and s, to understand the effect of distance/resolution/orientation and algorithm. For each TLS, we first present results for the center of sphere D and then discuss results for the center of the contrast target for the different cases shown in table 1. The variation of the sphere center across the different cases listed in table 1 is important to monitor because it represents our ability in establishing the coordinate system. If the variation in the contrast target center is much larger than that of the sphere, we can conclude that variation is in fact due to the algorithm and/or the distance/resolution/orientation combinations. On the other hand, if the variation in the contrast target center is not significantly larger than that of the sphere, we cannot conclusively state that the observed variation is due to the algorithm and/or the distance/resolution/orientation combinations. Response variables d and s are calculated from X and Y coordinates only as they are affected by the rotational orientation of the target. The Z coordinate is determined from the plane of the contrast target and is not affected by target rotation.

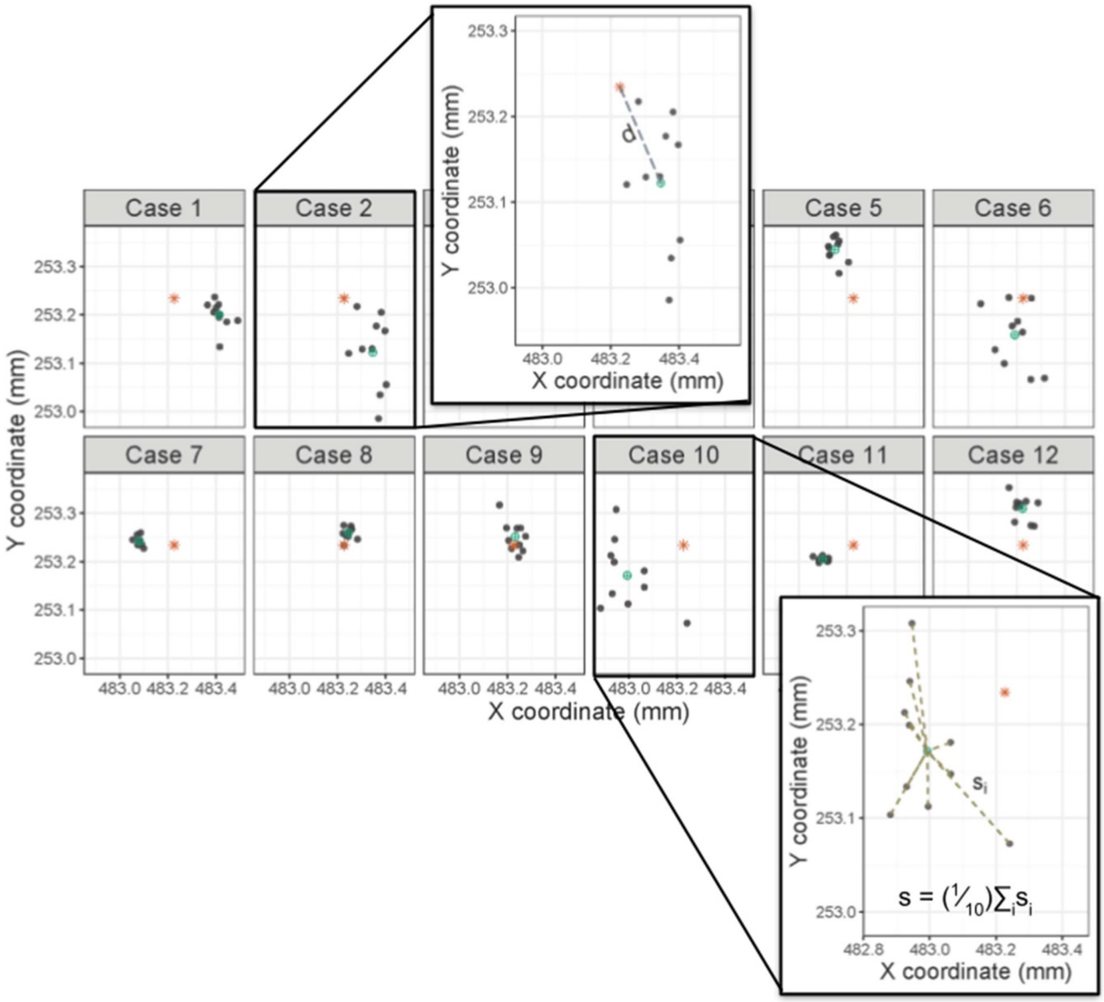

Figure 9. The overall center, $(\tilde{x}, \tilde{y})$, is shown in orange while the case center, $(\bar{x}_j, \bar{y}_j)$, is shown in blue. Note that the case center changes from case to case because it is the average coordinate for that case. Response variable d is a measure of the variation in the center coordinates across the different cases, i.e. it is the distance between the blue and orange dots. Response variable s is a measure of the variation in the center coordinates within a given case, i.e. it is the average distance between the 10 centers and the case center for a given case.

4.1. Calculation of the response variables

We first describe the calculation of the two response variables d and s for the sphere. For a given TLS, let (x_{ij}, y_{ij}) denote the sphere center coordinates for repeat i of case j, $i = 1, \ldots, 10; j = 1, \ldots, 12$. We calculated the median X and median Y coordinates, $(\tilde{x}, \tilde{y})$, which we will refer to as the 'overall center'. The overall center is shown as the orange dot in figure 9 for sphere D using the data from TLS A as an example. This center is determined from the 120 estimates of the center coordinates $(1, \ldots, 10; j = 1, \ldots, 12;)$. Next, we calculated the center coordinates for the 12 different cases as the average X and Y coordinates from the 10 replicate scans, which we refer to as the 'case center'. These are shown as the blue dots in figure 9. Let $(\bar{x}_j, \bar{y}_j)$ denote the case center for the jth case.

Inter-case variation *d*: This is defined as the offset distance between a case center and the overall center, given by

$$d_j = \sqrt{\left(\bar{x}_j - \tilde{x}\right)^2 + \left(\bar{y}_j - \tilde{y}\right)^2}. \quad (2)$$

This is shown in figure 9 for case 2.

Intra-case variation *s*: This is defined as the average offset distance from the case center within a set of 10 replicate scans for a given case. To evaluate this variable, for each case, we first calculated the offset distance between each center coordinate and its case center,

$$s_{ij} = \sqrt{\left(x_{ij} - \bar{x}_j\right)^2 + \left(y_{ij} - \bar{y}_j\right)^2}. \quad (3)$$

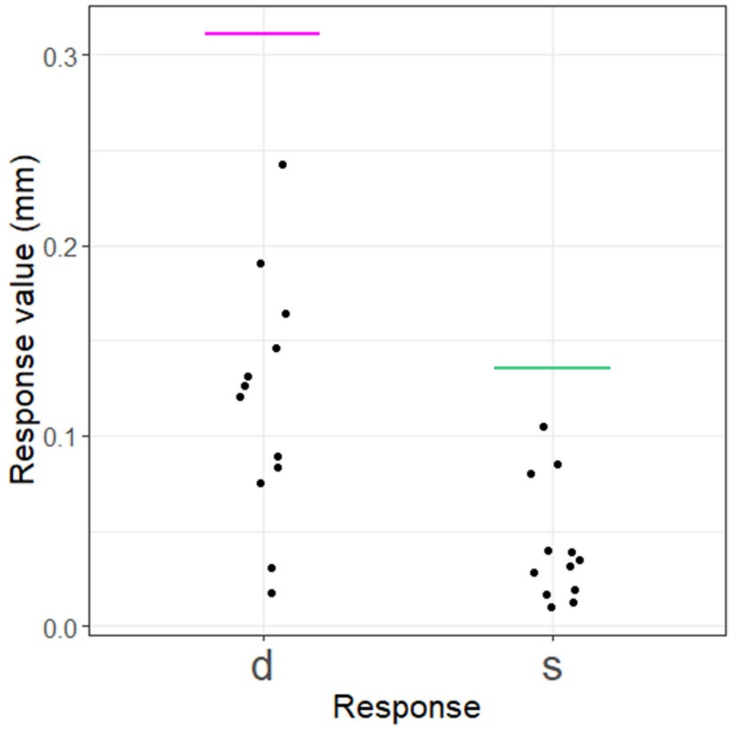

Figure 10. Response variables d and s calculated for sphere D for the 12 different cases. Thresholds are calculated as three standard deviations above the mean response. Points have been randomly staggered in the horizontal direction to minimize overlap.

We then calculated the average offset distance as

$$s_j = \frac{1}{10}\sum_{i=1}^{10} s_{ij}. \tag{4}$$

This is shown in figure 9 for case 10.

We performed similar calculations for the contrast target but because there are four algorithms, we estimated the response variables separately for each algorithm. To make comparisons between the OEM and custom algorithms easier, we only considered the worst performing custom algorithm for each case. To summarize, we estimated the following quantities from the data acquired:

- Sphere D: For each of the 12 cases, we estimated the inter-case variation d and intra-case variation s
- Contrast target OEM algorithm: for each of the 12 cases, we estimated the inter-case variation d and intra-case variation s
- Contrast target custom algorithms: for each of the 12 cases, and for each of the three custom algorithms, we estimated the inter-case variation d and intra-case variation s

When comparing the OEM algorithm to the custom algorithms for a given case, we chose the largest d and s from the three custom algorithms for that case, i.e. we only considered the worst performing custom algorithm and compared that to the OEM algorithm.

4.2. TLS A

The response variables d and s for sphere D are shown in figure 10. A threshold calculated as the sum of the mean and three times the standard deviation of the 12 values is also shown in the figure (purple line for d and green line for s). Response values for the contrast target that are larger than these thresholds can be reasonably attributed to the algorithm and/or the distance/resolution/orientation combinations.

In figure 11, we compare the performance of the OEM algorithm to the performance of the custom algorithm. Inter-case variation d for the OEM algorithm is plotted against inter-case variation d for the custom algorithm in figure 11(a). Intra-case variation s for the OEM algorithm is plotted against intra-case variation s for the custom algorithm in figure 11(b). A dashed diagonal line has been added to figure 11. Points that lie above the dashed line correspond to cases where the response value (either d

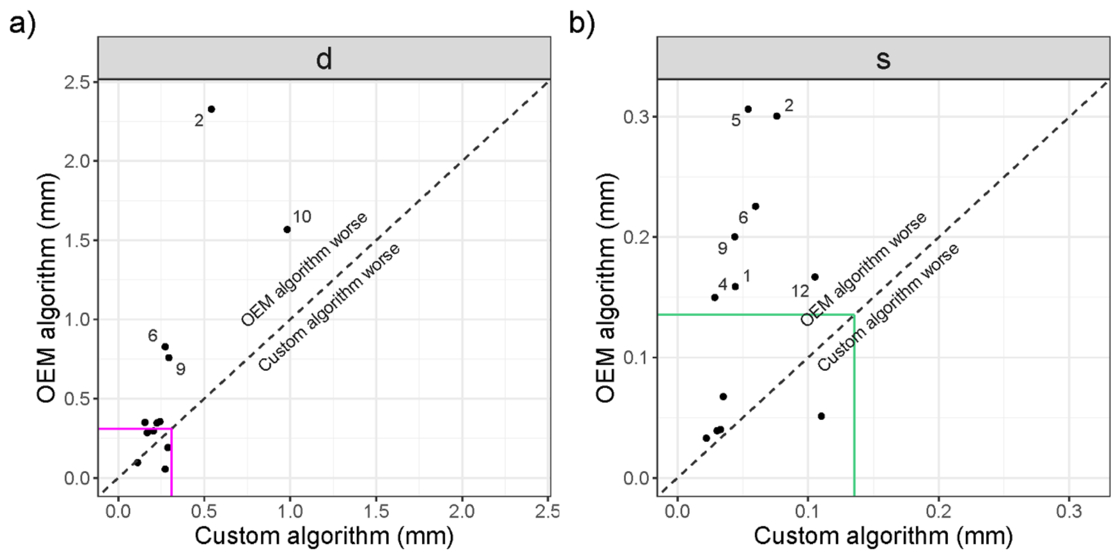

Figure 11. (a). Inter-case variation *d* for the OEM algorithm plotted against inter-case variation *d* for the custom algorithm, (b) intra-case variation *s* for the OEM algorithm plotted against intra-case variation *s* for the custom algorithm. Text annotation indicates case number.

or *s*) obtained from the OEM algorithm was higher (worse) than the response value obtained from the worst-performing custom algorithm. The purple and green lines in figure 11 correspond to the thresholds established from the sphere D values (figure 10), and text annotation identifies case numbers where response values were well above the corresponding threshold. From figure 11, values for *d* and *s* are generally larger for the OEM algorithm than for the worst performing custom algorithm indicating that the custom algorithms perform better. For example, *d* is approximately 2.2 mm for the OEM algorithm and 0.5 mm for the worst performing custom algorithm for case 2, which is a 77% improvement for that case. Intra-case variation *s* is approximately 0.3 mm for the OEM algorithm and 0.05 mm for the worst performing custom algorithm for case 5, which is an 83% improvement for that case.

We next consider the factors that potentially affected the performance of the OEM algorithm. The cases with the largest inter-case variation *d* for the OEM algorithm are cases 2, 10, 6, and 9 (figure 11(a)). The cases with the largest intra-case variation *s* for the OEM algorithm are cases 5, 2, 6, and 9. The *d* and *s* values for these cases are all above their corresponding thresholds. These cases all correspond to the 28 ppd setting indicating that the OEM algorithm performs poorly at low resolution. We further investigate the effect of different factors affecting the OEM algorithm through a factor analysis as described next.

The combinations for the 12 cases in table 1 correspond to a full factorial experiment on two-level factors (distance and resolution) and one three-level factor (angle). As such, we explore the effect of these factors on the OEM algorithm further by estimating the factorial effects, including the main factor effects and interaction effects, on both *d* and *s*. As specific hypotheses were not established *a priori* and data were collected without randomization, we restrict ourselves to the estimation and ranking of the factorial effects but refrain from conducting a formal statistical analysis to determine effect significance.

Table 2 defines the main factor effects for this analysis. For the two-level factors, distance and resolution, the factor effect is proportional to the change in the average experimental response (*d* or *s*) from the cases performed at the 'high' setting to the average response from the cases performed at the 'low' setting. For the three-level factor, angle, we use the linear-quadratic system to define the main and interaction effects. This system parameterizes the effect of angle through two orthogonal components: C1 compares the average response at a 90° roll angle to the average response at the lower two roll angles, while C2 compares the average response when roll angle is 67° to the average response when roll angle is 45°. In addition to the four main effects, five two-term interactions and two three-term interactions can be estimated from these data. Further information on estimating factor effects can be found in Wu and Hamada [28]

Figure 12 plots the magnitude of the factorial effects in descending order. The text annotation below each bar identifies the source of the effect using the letters defined in table 2. Single letters correspond to

Table 2. Factors and levels.

Factor	Low	High
A—distance	5 m	10 m
B—resolution	28 ppd	109 ppd
C1—angle	45° and 67°	90°
C2—angle	45°	67°

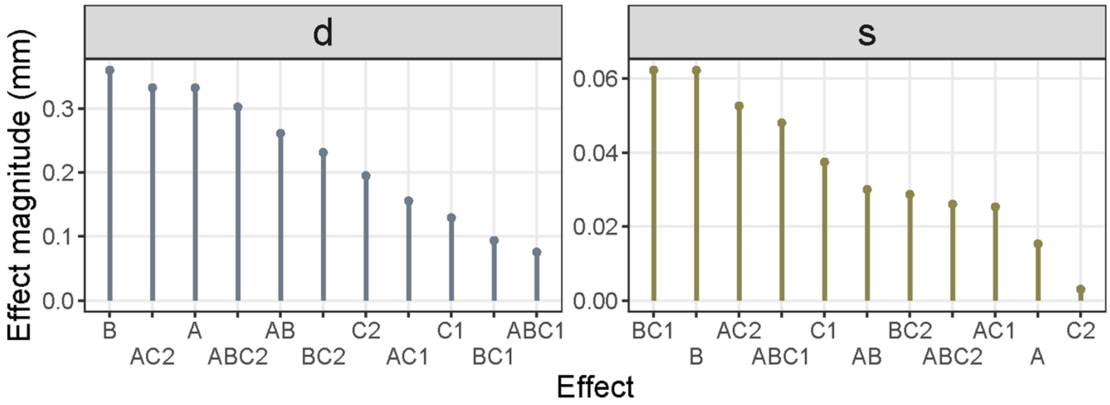

Figure 12. Absolute effect estimates from TLS A for the main and interaction effects from the factors listed in table 2, ranked by effect magnitude.

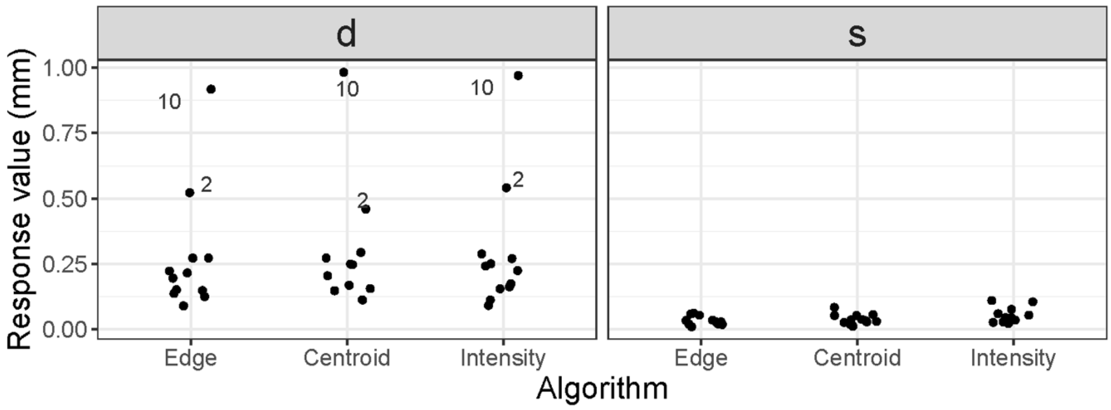

Figure 13. Distributions of d and s values from the three custom algorithms for TLS A. Text annotation identifies case numbers that produced large values. Points have been randomly staggered in the horizontal direction to minimize overlap.

a main factor effect, e.g. the largest effect on inter-case variation d is attributed to factor B, Resolution. Combination of letters correspond to interaction between factors, e.g. the BC1 interaction between resolution (factor B) and angle, specifically the largest roll angle compared to the other two (factor C1), has the largest effect on the intra-case variation s. Factor analysis also indicates that distance (factor A) by itself and in combination with angle (C2) has a large effect on inter-case variation d while the interaction between resolution (factor B) and angle (C1) has a large effect on intra-case variation s.

In many systems, the responses are driven by just a few effects. In such cases, when plotting the magnitude of the factorial effects there will be a clear distinction in bar heights. In figure 12, the height of the bars gradually decreases without an obvious 'elbow' point, which may be indicative that none of the effects studied here are truly significant. Further experimentation would be needed to be conducted to clarify the significance of these effects.

Finally, we compare the three custom algorithms. In figure 13, the d and s values from the 12 cases are plotted for each of the three custom algorithms. Text annotation has been added to identify certain case numbers that had large values. The distribution of values is very similar across the three algorithms, suggesting no noticeable difference in custom algorithm performance. All custom algorithms performed poorly for case 10, i.e. far distance, low resolution, and 90° target orientation.

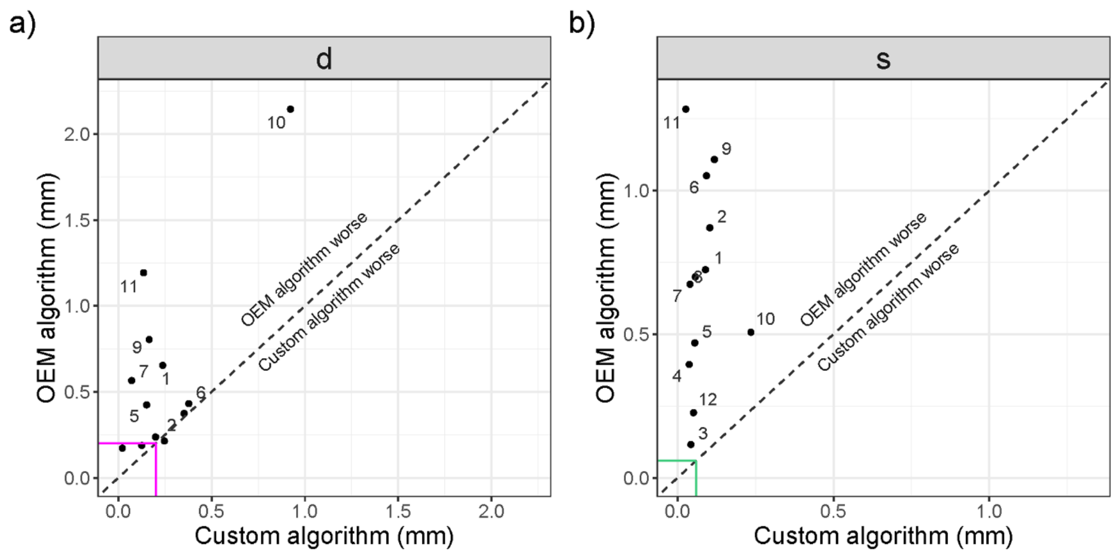

Figure 14. (a). Inter-case variation *d* for the OEM algorithm plotted against inter-case variation *d* for the custom algorithm, (b) intra-case variation *s* for the OEM algorithm plotted against intra-case variation *s* for the custom algorithm. Text annotation indicates case number.

4.3. TLS B

In figure 14, we compare the performance of the OEM algorithm to the performance of the custom algorithm for TLS B. As before, inter-case variation *d* for the OEM algorithm is plotted against inter-case variation *d* for the custom algorithm in figure 14(a). Intra-case variation *s* for the OEM algorithm is plotted against intra-case variation *s* for the custom algorithm in figure 14(b). The purple and green lines in figure 14 correspond to the thresholds established from the sphere D value for this TLS, and text annotation identifies case numbers where response values were well above the corresponding threshold. From figure 14, values for *d* and *s* are generally larger for the OEM algorithm than for the worst performing custom algorithm indicating that the custom algorithms perform better. For example, *d* is approximately 2.2 mm for the OEM algorithm and 0.9 mm for the worst performing custom algorithm for case 10, which is a 59% improvement for that case. Intra-case variation *s* is approximately 1.3 mm for the OEM algorithm and 0.1 mm for the worst performing custom algorithm for case 11, which is an 92% improvement for that case.

We next consider the factors that potentially affected the performance of the OEM algorithm. Case 10 (10 m, 28 ppd, 90° orientation combination) produced the largest inter-case variation *d*, which is significantly larger than the threshold (purple line). Numerous cases produced large intra-case variation *s*. The four largest values were for cases 11, 9, 6, 2, and 1, all of which are significantly larger than the corresponding threshold (green line). To better understand the factors contributing to these large values, we consider the plot in figure 15 which shows the magnitude of the factorial effects in descending order. The largest effect on inter-case variation *d* is attributed to factor C1, target orientation. That is, the 90° target orientation produced values for inter-case variation *d* that is noticeably different from the values for 45° and 67° orientation. The largest effect on intra-case variation *s* is attributed to factor AC1. That is, far distance (10 m) and 90° target orientation produced values for intra-case variation *s* that were noticeably different than for the other cases.

In figures 16, the *d* and *s* values from the 12 cases are plotted for each of the three custom algorithms. There is no noticeable difference in custom algorithm performance. All custom algorithms performed poorly for case 10, i.e. far distance (10 m), low resolution (28 ppd), and 90° target orientation.

4.4. TLS C

We compare the performance of the OEM algorithm to the performance of the custom algorithm in figure 17 for TLS C. Values for response variables *d* and *s* are generally comparable between the OEM algorithm and the worst performing custom algorithm. These values are all within the threshold for this TLS, except for case 10 (10 m, 28 ppd, 90° orientation combination), indicating that the contrast

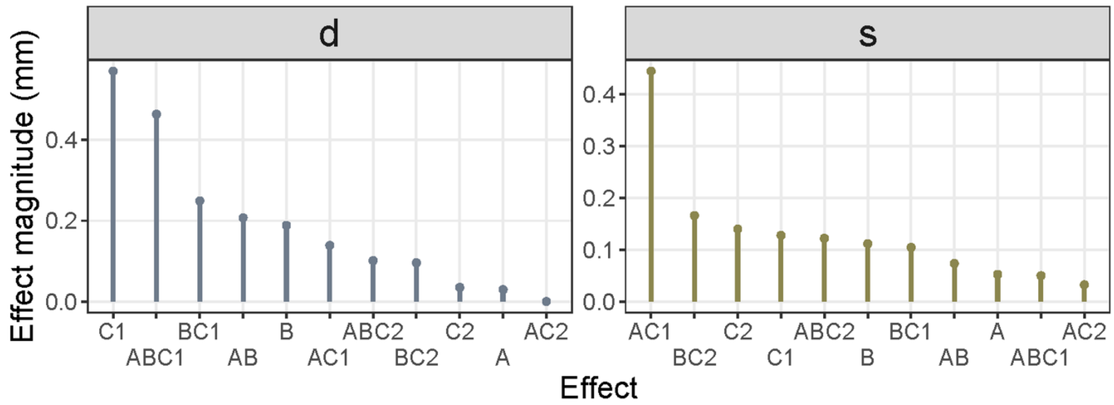

Figure 15. Absolute effect estimates from TLS B for the main and interaction effects from the factors listed in table 2, ranked by effect magnitude.

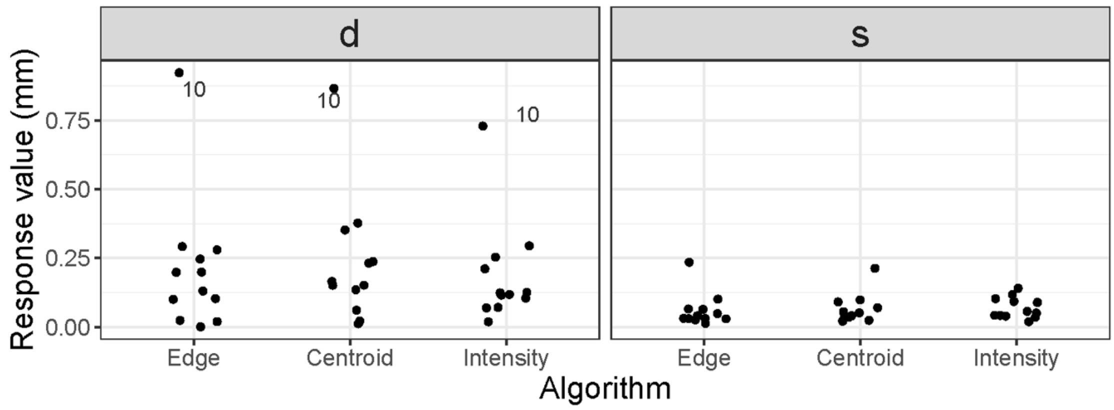

Figure 16. Distributions of *d* and *s* values from the three custom algorithms for TLS B. Text annotation identifies case numbers that produced large values. Points have been randomly staggered in the horizontal direction to minimize overlap.

target algorithms perform comparably with sphere fitting in most cases. Case 10 produced the largest inter-case variation *d* and the largest intra-case variation *s* for both the OEM and custom algorithms with the OEM performing marginally better than the worst performing custom algorithm.

Because case 10 was the only case that produced *d* and *s* values larger than their corresponding thresholds, we do not analyze the effect of various factors such as distance/resolution/orientation. Figure 18 shows a comparison across the three custom algorithms. As before, there is no noticeable difference in custom algorithm performance. All custom algorithms performed poorly for case 10, i.e. far distance, low resolution, and 90° target orientation.

5. Conclusions

Contrast targets are commonly used in conjunction with TLSs to either evaluate the performance of the TLS or to register scans from different locations. These targets have alternating black and white geometries (typically, rectangles or triangles), the point of intersection being the center of the target. In this paper, we explored the effect of rotational orientation of the target (rotation in the plane of the target) on the center coordinate. We considered three TLSs, two target distances, two resolutions, three rotational orientations, and four algorithms (one from the OEM, and three custom developed) in our study. Our study was conducted on a specially built artifact comprising four spheres and a contrast target that allowed us to monitor the center of the contrast target in a coordinate system built using the center of three spheres. Spheres centers are not influenced by the factors considered in this study, therefore the coordinate system established using spheres are stable across the different cases considered. For both the fourth sphere (sphere D) and the contrast target, we monitored two response variables for the 12 cases

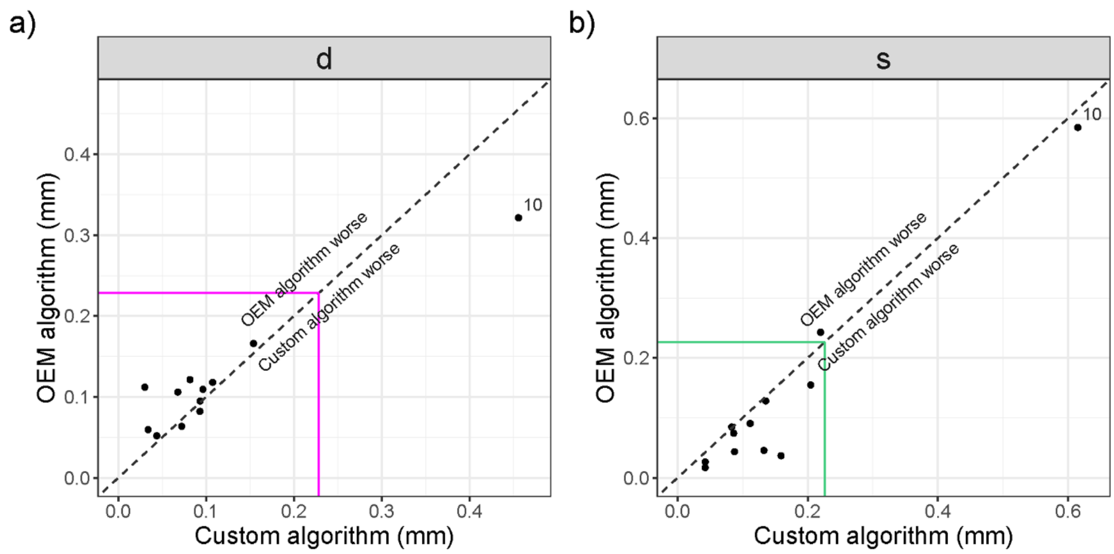

Figure 17. (a). Inter-case variation *d* for the OEM algorithm plotted against inter-case variation *d* for the custom algorithm, (b) intra-case variation *s* for the OEM algorithm plotted against intra-case variation *s* for the custom algorithm. Text annotation indicates case number.

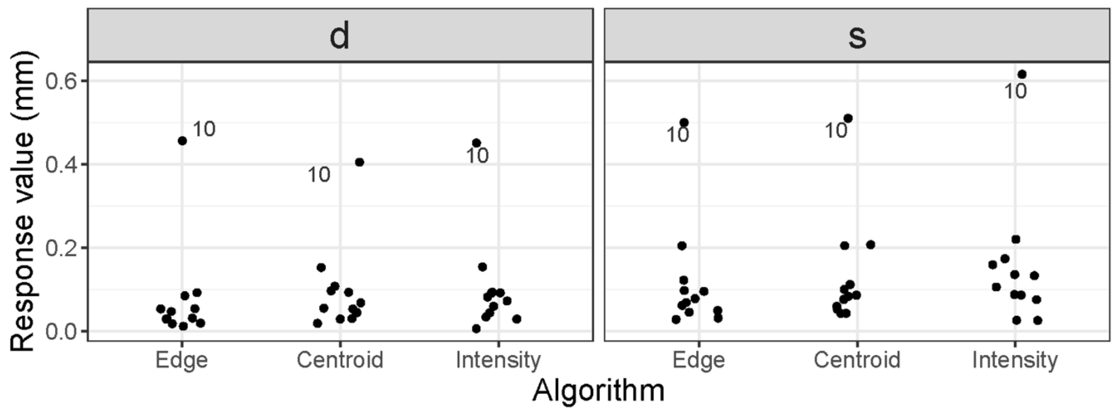

Figure 18. Distributions of *d* and *s* values from the three custom algorithms for TLS C. Text annotation identifies case numbers that produced large values. Points have been randomly staggered in the horizontal direction to minimize overlap.

(different combinations of distance/resolution/target-orientation) we considered—the inter-case variation *d* and the intra-case variation *s*. We note the following.

For TLS A:

- Response variables *d* and *s* for the contrast target were significantly larger than the threshold (determined from sphere D) for some cases, indicating a problem with distance/resolution/orientation and/or the algorithm.
- Custom algorithms generally performed better (smaller *d* and *s* values) than the OEM algorithm. One case showed a 77% improvement in *d* and an 83% improvement in *s*.
- With regards to the OEM algorithm, low resolution (28 ppd) produced large values for *d* and *s*, as large as 2 and 0.3 mm, respectively, for one of the cases. In addition, target rotational orientation in combination with distance and resolution also affected *d* and *s* values.
- All three custom algorithms performed comparably.

For TLS B:

- Response variables *d* and *s* for the contrast target were significantly larger than the threshold (determined from sphere D) for some cases, indicating a problem with distance/resolution/orientation and/or the algorithm.
- Custom algorithms generally performed better (smaller *d* and *s* values) than the OEM algorithm. One case showed a 59% improvement in *d* value and a 92% improvement in *s* value.
- With regards to the OEM algorithm, 90° target orientation produced large values for *d* while a combination of distance (10 m) and 90° orientation produced large values for *s*. These values were as large as 2 and 1.3 mm, respectively, for certain cases.
- All three custom algorithms performed comparably.

For TLS C:

- Response variables *d* and *s* for the contrast target were within the threshold (determined from sphere D) for all cases except for case 10.
- Case 10 produced the largest inter-case variation *d* and the largest intra-case variation *s* for both the OEM and custom algorithms with the OEM performing marginally better than the worst performing custom algorithm. These values were as large as 0.3 and 0.6 mm, respectively, for the OEM algorithm.

In summary, the rotational orientation of the target, especially at low resolution and far distance is an important factor to consider when using contrast targets in the scene of a TLS scan. Because the algorithm plays a key role, we recommend users discuss appropriate target orientation with the TLS manufacturer prior to placing them in the scene. For our custom algorithms, target orientation of 45° or 67° is a better choice than the 90° orientation.

Acknowledgments

The authors thank members of the OSAC working group for their feedback and Octavio Icasio Hernandez and Jack Prothero at NIST for reviewing the paper.

Data availability statement

The data cannot be made publicly available upon publication because they are not available in a format that is sufficiently accessible or reusable by other researchers. The data that support the findings of this study are available upon reasonable request from the authors.

Disclaimer

Commercial equipment and materials may be identified in order to adequately specify certain procedures. In no case does such identification imply recommendation or endorsement by the National Institute of Standards and Technology, nor does it imply that the materials or equipment identified are necessarily the best available for the purpose.

Author contributions

Bala Muralikrishnan 0000-0002-0313-9708
Conceptualization (equal), Data curation (equal), Formal analysis (equal), Investigation (equal), Methodology (equal), Software (equal), Validation (equal), Visualization (equal), Writing – original draft (equal), Writing – review & editing (equal)

Aum Shah 0009-0002-8449-4636
Data curation (equal), Formal analysis (equal), Investigation (equal), Methodology (equal), Software (equal), Writing – original draft (equal)

Mary Gregg 0000-0003-2991-6939
Formal analysis (equal), Software (equal), Writing – review & editing (equal)

Meghan Shilling 0009-0004-0962-428X
Conceptualization (equal), Data curation (equal), Formal analysis (equal), Investigation (equal), Methodology (equal), Writing – original draft (equal), Writing – review & editing (equal)

Vincent Lee 0000-0002-2953-6322
Data curation (equal), Investigation (equal), Writing – review & editing (equal)

Braden Czapla 0000-0002-3248-2134
Conceptualization (equal), Data curation (equal), Formal analysis (equal), Investigation (equal), Methodology (equal), Software (equal), Writing – review & editing (equal)

References

[1] Staiger R 2011 *10 years of terrestrial laser scanning—technology, systems and applications* (GEO-Siberia) pp 26–29
[2] Shan J and Toth C K (eds) 2009 *Topographic Laser Ranging and Scanning: Principles and Processing* (CRC Press)
[3] Aryan A, Bosché F and Tang P 2021 Planning for terrestrial laser scanning in construction: a review *Autom. Constr.* **125** 103551
[4] Wu C, Yuan Y, Tang Y and Tian B 2022 Application of terrestrial laser scanning (TLS) in the architecture, engineering and construction (AEC) industry *Sensors* **22** 265
[5] Shen N, Wang B, Ma H, Zhao X, Zhou Y, Zhang Z and Xu J 2023 Review of terrestrial laser scanning (TLS)-based technologies for deformation monitoring in engineering *Measurement* **223** 113684
[6] Mukupa W, Roberts G W, Hancock C M and Al-Manasir K 2017 A review of the use of terrestrial laser scanning application for change detection and deformation monitoring of structures *Surv. Rev.* **49** 353
[7] Kekeç B, Bilim N, Karakaya E and Ghiloufi D 2021 Applications of terrestrial laser scanning (TLS) in mining: a review *Turk. Lidar J* **3** 31–38
[8] Mohammed Oludare I and Pradhan B 2016 A decade of modern cave surveying with terrestrial laser scanning: a review of sensors, method and application development *Int. J. Speleol.* **45** 71–88
[9] Wang W, Zhao W, Huang L, Vimarlund V and Wang Z 2014 Applications of terrestrial laser scanning for tunnels: a review *J. Traffic Transp. Eng.* **1** 325–37
[10] Rashidi M, Mohammadi M, Sadeghlou Kivi S, Mehdi Abdolvand M, Truong-hong L and Samali B 2020 A decade of modern bridge monitoring using terrestrial laser scanning: review and future directions *Remote Sens.* **12** 3796
[11] Demol M *et al* 2022 Estimating forest above-ground biomass with terrestrial laser scanning: current status and future directions *Methods Ecol. Evol.* **13** 1628–39
[12] Liu J, Azhar S, Willkens D and Li B 2023 Static terrestrial laser scanning (TLS) for heritage building information modeling (HBIM): a systematic review *Virtual Worlds* **2** 90–114
[13] Galvin R 2020 *Crime Scene Documentation—Preserving the Evidence and the Growing Role of 3D Laser Scanning* (CRC Press) (https://doi.org/10.4324/9781003128465)
[14] Maisano D A, Mastrogiacomo L, Franceschini F, Capizzi S, Pischedda G, Laurenza D, Gomiero G and Manca G 2023 Dimensional measurements in the shipbuilding industry: on-site comparison of a state-of-the-art laser tracker, total station and laser scanner *Prod. Eng.-Res. Dev.* **17** 625–42
[15] Muralikrishnan B, Lu X, Gregg M, Shilling M and Czapla B 2025 A method to evaluate orientation-dependent errors in the center of contrast targets used with terrestrial laser scanners *Sensors* **25** 505
[16] Chow J C K, Teskey W F and Loves J 2011 In-situ self-calibration of terrestrial laser scanners and deformation analysis using both signalized targets and intersection of planes for indoor applications *Proc. 14th FIG Symp. on Deformation Measurements and Analysis, 5th IAG Symp. on Geodesy for Geotechnical and Structural Engineering, and 2nd Int. Workshop on Spatial Information Technologies for Monitoring the Deformation of Large-Scale Man-Made Linear Features (2–4 November 2011)* (Hong Kong) pp 2–16
[17] Ge X and Wunderlich T 2015 Target identification in terrestrial laser scanning *Surv. Rev.* **47** 129–40
[18] Rachakonda P, Muralikrishnan B and Sawyer D 2019 Metrological evaluation of contrast target center algorithm for terrestrial laser scanners *Measurement* **134** 15–24
[19] Abmayr T, Härtl F, Hirzinger G, Burschka D and Fröhlich C 2008 A correlation based target finder for terrestrial laser scanning *J. Appl. Geod.* **2** 131–7
[20] Liang Y B, Zhan Q M, Che E Z, Chen M W and Zhang D L 2014 Automatic registration of terrestrial laser scanning data using precisely located artificial planar targets *IEEE Geosci. Remote Sens. Lett.* **11** 69–73
[21] Yi C, Xing H, Wu Q, Zhang Y, Wei M, Wang B and Zhou L 2018 Automatic detection of cross-shaped targets for laser scan registration *IEEE Access* **6** 8483–500
[22] Fryskowska A 2019 An improvement in the identification of the centres of checkerboard targets in point clouds using terrestrial laser scanning *Sensors* **19** 938
[23] Moh Goo J, Li J, Wicaksono D and Boehm J 2025 Checkerboard target measurement in unordered point clouds with coloured ICP *Int. Arch. Photogramm. Remote Sens. Spat. Inf. Sci.* **XLVIII-G-2025** 529–34
[24] Janßen J, Medic T, Kuhlmann H and Holst C 2019 Decreasing the uncertainty of the target center estimation at terrestrial laser scanning by choosing the best algorithm and by improving the target design *Remote Sens.* **11** 845
[25] OSAC website (available at: www.nist.gov/adlp/spo/organization-scientific-area-committees-forensic-science) (Accessed 18 June 2025)

[26] Gregg M, Muralikrishnan B and Shilling M 2026 Toward a documentary standard for performance testing of terrestrial laser scanners used in forensic practice: a statistical procedure to assess change in instrument precision *J. Forensic Sci.* **71** 1023–31

[27] Muralikrishnan B, Shilling M, Gregg M, Lee V, Keller J, Casey E, Liscio E, O'Neil B, Russ M and Terpstra T 2025 Report on the May 2025 NIST measurement week: realization of an OSAC draft interim performance assessment for terrestrial laser scanners used by law enforcement agencies *NISTIR 8583* (https://doi.org/10.6028/NIST.IR.8583)

[28] Wu C J and Hamada M S 2021 *Experiments: Planning, Analysis, and Optimization* (Wiley)